Langmuir

Article

pubs.acs.org/Langmuir

In Situ Modulation of Cell Behavior via Smart Dual-Ligand Surfaces

Abigail Pulsipher,[†] Sungjin Park,[†] Debjit Dutta,[†] Wei Luo,[†,‡] and Muhammad N. Yousaf*[,†,‡]

[†]Department of Chemistry, University of North Carolina at Chapel Hill, Chapel Hill, North Carolina 27599-3290, United States
[‡]Department of Chemistry and Biology, York University, Toronto, Ontario M3J 1P3, Canada

Supporting Information

ABSTRACT: Due to the highly complex nature of the extracellular matrix (ECM), the design and implementation of dynamic, stimuli-responsive surfaces that present well-defined ligands and serve as model ECM substrates have been of tremendous interest to biomaterials, biosensor, and cell biology communities. Such tools provide strategies for identifying specific ligand−receptor interactions that induce vital biological consequences. Herein, we report a novel dual-ligand-presenting surface methodology that modulates dynamic ECM properties to investigate various cell behaviors. Peptides PHSRN, cRGD, and KKKTTK, which mimic the cell- and heparan sulfate-binding domains of fibronectin, and carbohydrates Gal and Man were combined with cell adhesive RGD to survey possible synergistic or antagonist ligand effects on cell adhesion, spreading, growth, and migration. Soluble molecule and enzymatic inhibition assays were also performed, and the levels of focal adhesion kinase in cells subjected to different ligand combinations were quantified. A redox-responsive trigger was incorporated into this surface strategy to spontaneously release ligands in the presence of adhered cells, and cell spreading, growth, and migration responses were measured and compared. The identity and nature of the dual-ligand combination directly influenced cell behavior.

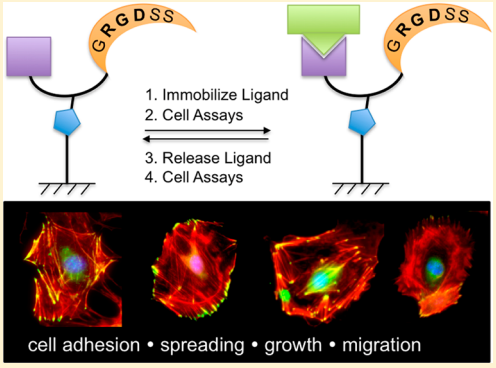

INTRODUCTION

The extracellular matrix (ECM) is a highly dynamic, insoluble aggregate of collagens, proteoglycans, structural glycoproteins, and elastin that provides structural support for the adhesion, growth, differentiation, migration, and survival of mammalian cells.[1−3] Improper cell attachment and migration have been implicated in cancer cell metastasis and other diseased states, including fibrosis.[4−7] For a cell to undergo migration, it must first adhere to another cell or the ECM through cell surface receptor−ligand interactions.[8] Integrins and syndecans, which are transmembrane proteins, represent the most common cell surface receptor families that facilitate cell adhesion to the ECM and transduce extra- and intracellular signals.[9−11]

Fibronectin (FN) is a predominant ECM glycoprotein that contains three homologous globular domains—types I, II, and III—and possesses a number of interaction sites for both integrins and syndecans.[12] As such, FN plays an important role in cell adhesion, growth, migration, and differentiation and is critical to cellular processes, including embryogenesis and tissue repair.[13] A number of cell types bind to FN regions that span the 8th to 10th type III ($FNIII_{8-10}$) cell-binding domain. Arg-Gly-Asp (RGD), found in $FNIII_{10}$, was identified as the minimal cell attachment sequence of $\alpha5\beta1$ and $\alpha V\beta3$ integrin recognition.[14] A synergy site that presents Phe-His-Ser-Arg-Asn (PHSRN) was then identified in $FNIII_9$ and shown to enhance FN's association with $\alpha5\beta1$ integrins, mediating cell adhesion and migration.[15−18] RGD and PHSRN are presented on the same plane of FN, connected by a flexible 30-40 Å linker.[19] Spatial orientation and positioning of these signals are crucial for inducing synergistic effects on cell adhesion and migration. Furthermore, conflicting reports of whether PHSRN alone is capable of supporting cell adhesion have been a topic of debate over the past decade.[15−18]

Although $\alpha5\beta1$ and $\alpha V\beta3$ integrins serve as the primary cell surface receptors that mediate adhesion, syndecan-4, a transmembrane heparan sulfate proteoglycan (HSPG), is a coreceptor for FN.[20,21] A heparan sulfate (HS) binding domain spans $FNIII_{12-14}$. Simultaneous interactions of syndecan-4 and $\alpha5\beta1$ integrin with $FNIII_{12-14}$ and $FNIII_{8-10}$, respectively, induces downstream signaling events, leading to the activation of focal adhesion kinase (FAK) and extracellular signal-regulated kinase (ERK) with subsequent complete cell attachment and enhanced spreading via focal adhesion complex (FAC) formation.[12,20,21] A few HS binding domain mimics have been tested; however, similar to the synergistic effect of RGD and PHSRN on cell adhesion, these small molecules or sequences are less efficient in promoting cell attachment alone. Such mimics contain the sequence B-B-B-X-X-B, where B is a basic amino acid (e.g., Arg or Lys) and X is a hydropathic amino acid (e.g., Ser, Tyr, or Thr).[22−24] Conflicting hypotheses regarding the role of HS binding sequences on virus attachment have been reported. The Lys-Lys-Thr-Lys (KKTK) motif, found in the human adenovirus (hAd) fiber shaft, serves a minimal role in binding HSPGs but is significant to virus

Received: September 3, 2014
Revised: October 13, 2014
Published: November 6, 2014

   dx.doi.org/10.1021/la503521x | *Langmuir* 2014, 30, 13656−13666

infection and trafficking into the nucleus.[25] Two separate works demonstrated that different hAd types, which lacked the KKTK motif, were able to attach and infect hepatic cells in vivo.[26,27] However, little is known concerning the role of HS binding sequences on cell adhesion and migration and its possible synergistic effects, if any, with RGD.

Due to the complex nature of the ECM, identifying all the diverse small molecules and ligand−cell surface receptor combinations that induce specific biochemical processes remains challenging.[28,29] Rather than performing in vitro studies with large native FN (~440 kDa), which is purified from blood plasma and tends to denature or adsorb in unnatural orientations and conformations on surfaces, researchers have sought to discover alternative approaches. As such, tremendous effort has been extended to creating model substrates that mimic the ECM using structurally well-defined, decoupled biomolecules, including RGD and PHSRN.[18,30] Such surfaces enable the spatial and temporal presentation of well-defined ligands for the interrogation of biospecific ligand−cell surface receptor interactions, providing great tools for applications in cell biology, biotechnology, and tissue engineering.

Over the past decade, self-assembled monolayers (SAMs) of alkanethiolates on gold have proven to be smart, dynamic, and stimuli-responsive model surfaces for a number of cell biological investigations.[31−34] "Dynamic" refers to the in situ control of cell behavior in response to an applied external stimulus. Liu et al. demonstrated that cells attach to the *E* isomer of RGD-conjugated azobenzene SAMs.[35] However, when irradiated with UV light, azobenzene adopted the *Z* conformation, masking RGD, and the cells detached. Using a photodeprotection strategy, Lee and colleagues selectively exposed and conjugated SAM regions with RGD to probe cell adhesion, polarization, and migration behaviors.[36] Moreover, Lamb and Yousaf reported a dynamic and switchable strategy based on electrochemically controlled hydroquinone (HQ) SAMs, in which the affinity of RGD ligands was altered.[37] Upon the application of a specific oxidative (Ox) or reductive (Red) electrochemical potential, the HQ could be turned "off" and "on" to reveal or hide RGD ligands for cell attachment studies. Furthermore, in a mild, reducing environment, HQ has been shown to release its covalently bound ligand in the presence of living cells for subsequent immobilization and release cycles with negligible affects on cell behavior and viability.[38,39] In vivo, ECM proteins and cell surfaces are constantly being remodeled and modified, where ligands are subjected to different compositions and orientations for biomolecular recognition. Therefore, model substrates that can mimic and modulate the highly evolving ECM would serve as great analytical tools, providing insight into the mechanisms of cell adhesion and migration in real time.

Herein, we report a dynamic, redox-responsive strategy to immobilize and release ligands in the presence of cells for cell adhesion, spreading, morphology, and migration studies (Figure 1). Electrochemistry enables the complete quantitative control over ligand density and provides a dynamic molecular switch for the combinatorial discovery of ligand effects. Two bioothogonal coupling methodologies, click and oxime chemistry, were incorporated, and an HQ- and azide (N_3)-functionalized RGD peptide (HQ-RGD) was synthesized to modulate the ECM. Commercially available lysine-N_3 and derivatized glycine-HQ were incorporated into Ser-Ser-Asp-Gly-Arg-Gly-C_6 linker via solid-phase peptide synthesis to

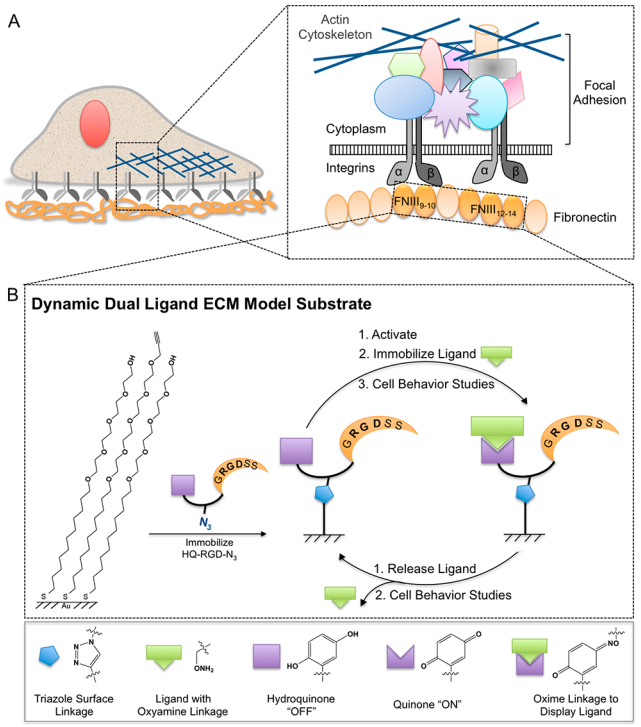

Figure 1. Simplified schematics of (A) cell adhesion to ECM protein FN via integrin interaction with $FNIII_{9-10}$ cell-binding domains, cytoplasmic proteins, and the actin cytoskeleton to form a FAC and (B) a dynamic dual-ligand ECM model substrate. SAMs of alkyne-terminated tetra(ethylene glycol) (alkyne-EG_4SH) and tetra(ethylene glycol)-terminated (EG_4SH) alkanethiols are generated on gold substrates and reacted with hydroquinone- and azide-functionalized cell adhesive peptide RGD (HQ-RGD-N_3). HQ is considered "off" and can be turned "on" for oxyamine (OA) ligand conjugation by electrochemical oxidation. Ligands that are functionalized with OA groups (i.e., peptides, KKKTTK-OA, PHRSN-OA, RGD-OA, cRGD-OA, and sugars, Man-OA, Gal-OA) react and conjugate to Q-presenting surfaces under physiological conditions. Cells are cultured and observed on surfaces displaying cell adhesive RGD and variable biomolecule. In situ electrochemical reduction dynamically releases the variable biomolecule, and cellular response to this environmental change is monitored.

generate K(N_3)-C_6 linker-G(HQ)GRGDSS, where the N_3 moiety is conjugated to alkyne-terminated SAMs via click chemistry and the HQ serves as a conjugation site for a variety of oxyamine-containing ligands. Synergy peptide PHSRN, high affinity cyclic RGD (cRGD), putative HS-binding sequence KKKTTK, and monosaccharides galactose (Gal) and mannose (Man) were functionalized with oxyamine groups and surveyed for potential synergistic or antagonistic effects with cell-adhesive RGD. Fibroblasts (Fbs) were seeded to the different ECM mimics substrates, with or without HQ-RGD, and the number of attached cells, spreading area, morphologies, and migration rates were tabulated. Inhibition and competitive binding studies were also performed in which soluble FN, cRGD, and HS were added. Chondroitinase ABC and heparinase I and II were also delivered to Fbs in culture to determine whether HS-binding KKKTTK exhibited a synergistic effect on cell adhesion and spreading. FAK protein levels were also detected and quantified. Furthermore, the ligands were released in the presence of cells, providing the dynamic component to our system, and cell adhesion, morphology, and migration rates were again examined. To our knowledge, this is

dx.doi.org/10.1021/la503521x | *Langmuir* 2014, 30, 13656−13666

the first report that uses a density-controlled, bioorthogonal, and stimuli-responsive model ECM to probe ligand−cell surface integrin and syndecan interactions in situ. The ability to switch ligands for the combinatorial screening of synergistic of antagonistic ligand effects provides a platform that would be of tremendous significance to the biosensor and biomaterials research communities.

MATERIALS AND METHODS

Chemicals and Reagents. All chemicals and reagents were of analytical grade and used without further purification. Common chemicals were obtained from Fischer Scientific (Pittsburgh, PA) or Sigma-Aldrich (St. Louis, MO) unless specified. Rink amide 4-methylbenzylhydrylamine (MBHA) resin, amino acids [Fmoc-Arg-(Pbf)-OH, Fmoc-Asp(OtBu)-OH, Fmoc-Gly-OH, Fmoc-Ser(tBu)-OH, Fmoc-Thr(tBu)-OH, Fmoc-Lys(Boc)-OH, and Fmoc-Lys(N_3)-OH], Boc-aminooxyacetic acid, Fmoc-ε-Ahx-OH, and HBTU were purchased from Anaspec (San Jose, CA). Antibodies antipaxillin and antivinculin and Cy-2 goat anti-mouse IgG were purchased from BD Biosciences (San Jose, CA) and Jackson ImmunoResearch Laboratories, Inc. (West Grove, PA), respectively. Fluorescent dyes DAPI and phalloidin and penicillin/streptomycin were obtained from Invitrogen (Carlsbad, CA). Fluorescence mounting medium was purchased from Dako (Carpinteria, CA). Swiss albino 3T3 mouse fibroblasts were obtained from the UNC-CH Tissue Culture Facility (Chapel Hill, NC). Heparan sulfate, heparinase I and II, and chondroitinase ABC were obtained from Sigma-Aldrich (St. Louis, MO).

Syntheses. Alkyne-terminated tetra(ethylene glycol) alkanethiol (alkyne-EG_4SH, **7**) was synthesized as previously reported.[40] Tetra(ethylene glycol)-terminated alkanethiol (EG_4SH, **8**) was prepared as previously described.[41] Rhodamine-oxyamine (Rhod-OA) was synthesized as previously demonstrated.[42] Galactose- and mannose-oxyamine (**5** and **6**, respectively) were also synthesized as previously reported.[43] Synthetic routes and a list of molecules are respectively shown in Schemes 1 and 2.

*1,4-Bis((tetrahydro-2H-pyran-2-yl)oxy)benzene (**A**).* To a solution of hydroquinone (6.0 g, 54.5 mmol) in tetrahydrofuran (THF, 40 mL) were added 3,4-dihydropuran (20.8 mL, 245.3 mmol, 4.5 equiv) and three drops of concentrated HCl (cat.). The mixture was stirred for 16 h at room temperature. The reaction contents were then diluted with ethyl acetate (EtOAc, 20 mL) and extracted with 1 M sodium bicarbonate (3 × 25 mL) and brine (1 × 25 mL) and concentrated to afford a white solid, **A**. The solid product was dried under vacuum for an additional 3 h (10.23 g, 67.4%). ^{1}H NMR (400 MHz, $CDCl_3$, δ): 1.58−1.67 (m, 6H, J = 36 Hz; $-CH_2-$), 1.85−1.88 (m, 4H, J = 12 Hz; $-CH_2-$), 2.00−2.03 (m, 2H, J = 8 Hz; $-CH_2-$), 3.60−3.62 (m, 2H, J = 8 Hz; $-CH_2-$), 3.96−3.98 (m, 2H, J = 8 Hz; $-CH_2-$), 5.32−5.34 (t, 2H, J = 7 Hz; −CH−), 7.00 (s, 4H; Ar−H).

*2,2′-((2-(6-Bromohexyl)-1,4-phenylene)bis(oxy))bis(tetrahydro-2H-pyran) (**B**).* To a stirring solution of **A** (3.0 g, 10.8 mmol) in dry THF (100 mL) at 0 °C was added *tert*-butyllithium (1.5 M in pentane, 10.1 mL, 13.0 mmol, 1.2 equiv) dropwise. After the base addition, a white precipitate formed. The mixture was stirred for 2 h at 0 °C and then warmed to room temperature for 3 h. 1,6-Dibromohexane (3.3 mL, 21.6 mmol, 2 equiv) was then added, and the reaction was stirred for 16 h to afford a pale yellow liquid. The mixture was then diluted with EtOAc (20 mL); extracted with $NH_4^+Cl^-$ (2 × 25 mL), H_2O (1 × 50 mL), and brine (1 × 50 mL); dried over $MgSO_4$; and concentrated to a pale yellow oil. Silica flash column chromatography (Hex/EtOAc/DCM, 8:1:1) was employed to purify **B** (2.4 g, 50.6%). ^{1}H NMR (400 MHz, $CDCl_3$, δ): 1.40−1.42, 1.46−1.47 (d × m, 4H, J = 8 Hz; $-CH_2-$), 1.49 (m, 8H; $-CH_2-$), 1.86−1.88 (m, 6H, J = 8 Hz; $-CH_2-$), 2.02 (m, 2H; $-CH_2-$), 2.60−2.62 (t, 2H, J = 8 Hz; $-CH_2-$), 3.41−3.44 (m, 2H, J = 12 Hz; $-CH_2-$), 3.61−3.62 (m, 2H, J = 4 Hz; $-CH_2-$), 3.96−3.99 (m, 2H, J = 12 Hz; $-CH_2-$), 5.31 (s, 2H; $-CH_2-$), 6.85−6.87 (m, 2H, J = 8 Hz; Ar−H), 7.02−7.04 (d, 1H, J = 8 Hz; Ar−H).

Scheme 1. Synthetic Scheme of HQ-RGD: (A) Solution Synthesis of Fmoc-glycine-HQ[a] and (B) Solid-Phase Peptide Synthesis of HQ-RGD Using MBHA Resin[b]

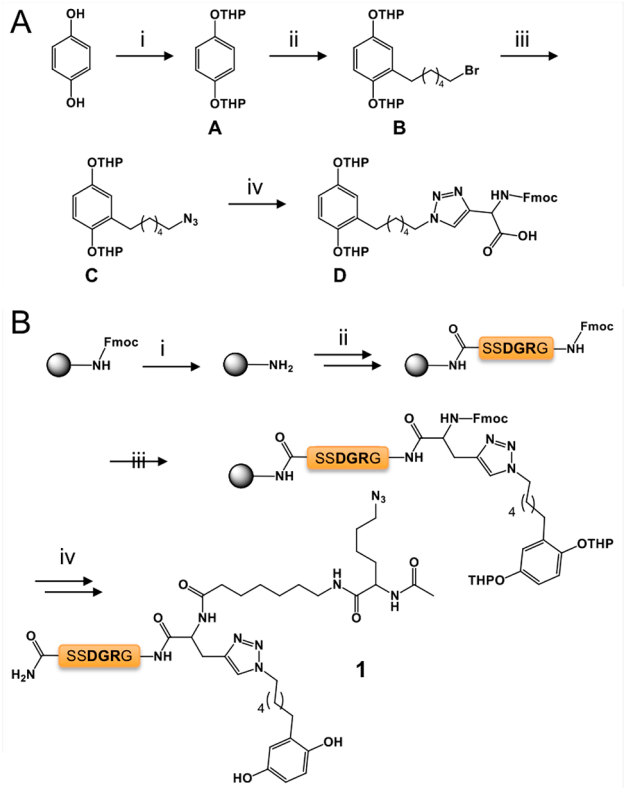

[a]Reagents and conditions: (i) DHP (4.5 equiv), HCl (cat.), THF, 16 h, 67.4%; (ii) *tert*-butyllithium (2 equiv), 1,6-dibromohexane (2 equiv), dry THF, 0−25 °C, 20 h, 50.6%; (iii) NaN_3 (1.5 equiv), DMF, 2 h, 80 °C; and (iv) Fmoc-propargylglycine (0.5 equiv), $CuSO_4·5H_2O$ (1.5 equiv), NaAsc (1.5 equiv), DMF/H_2O/EtOH (2:1:1), 12 h, 61.1%. [b]Reagents and conditions: (i) piperidine (20%); (ii) repetition of DIEA (3 equiv), HBTU (3 equiv), Fmoc-amino acid (SSDGRG, 3 equiv), DMF, then piperidine (20%); (iii) DIEA (3 equiv), HBTU (3 equiv), Fmoc-Gly-HQ (3 equiv), DMF, then piperidine (20%); (iv) DIEA (3 equiv), HBTU (3 equiv), Fmoc-C_6-linker (3 equiv), Fmoc-Lys-N_3 (3 equiv), piperidine (20%), acetic anhydride (10%), then TFA/H_2O (9.75/0.25, 2 h), ether suspension, centrifugation (2 × 2000 rpm, 10 min), dissolve and freeze in H_2O (10 mL), lyophilize. Overall yield of 54 mg, 65%.

*2,2′-((2-(6-Azidohexyl)-1,4-phenylene)bis(oxy))bis(tetrahydro-2H-pyran) (**C**).* To a solution of **B** (1.90 g, 4.32 mmol) in DMF at 80 °C was added sodium azide (0.56 g, 8.64 mmol, 2 equiv). The mixture was stirred for 2 h at 80 °C and was then cooled, diluted with DCM (20 mL), extracted with H_2O (3 × 25 mL), dried over $MgSO_4$, and concentrated to afford a pale yellow oil, **C** (1.72 g, 99.9%). No further purification was required. ^{1}H NMR (400 MHz, $CDCl_3$, δ): 1.38−1.39 (m, 4H, J = 4 Hz; $-CH_2-$), 1.59−1.61 (m, 10H, J = 8 Hz; $-CH_2-$), 1.84−1.85 (m, 4H, J = 4 Hz; $-CH_2-$), 1.95−1.97 (m, 2H, J = 8 Hz; $-CH_2-$), 2.57−2.61 (t, 2H, J = 16 Hz; $-CH_2-$), 3.23−3.26 (m, 2H, J = 12 Hz; $-CH_2-$), 3.56−3.61 (m, 2H, J = 16 Hz; $-CH_2-$), 3.86−3.96 (m, 2H, J = 40 Hz; $-CH_2-$), 5.28−5.30 (m, 2H, J = 8 Hz; $-CH_2-$), 6.80−6.82 (m, 2H, J = 8 Hz; Ar−H), 6.99−7.01 (d, 1H, J = 8 Hz; Ar−H).

*2-((((9H-Fluoren-9-yl)methoxy)carbonyl)amino)-3-(1-(6-(2,5-bis-((tetrahydro-2H-pyran-2-yl)oxy)phenyl)hexyl)-1H-1,2,3-triazol-4-yl)-propanoic Acid (Fmoc-Gly(HQ), **D**).* To a solution of **C** (1.64 g, 4.51 mmol, 2 equiv) and Fmoc-propargylglycine (0.76 g, 2.26 mmol) in DMF (20 mL) and EtOH (5 mL) was added a solution of $CuSO_4·5H_2O$ (0.85 g, 3.38 mmol, 1.5 equiv) and sodium ascorbate (0.67 g,

dx.doi.org/10.1021/la503521x | Langmuir 2014, 30, 13656−13666

Scheme 2. List of Molecules and Surface Groups Used in This Study[a]

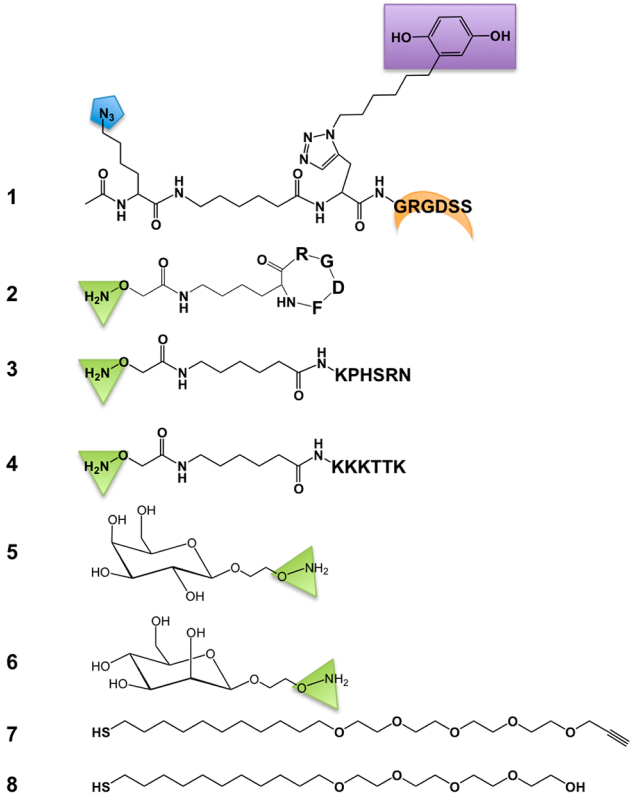

[a]The following molecules are depicted: (1) hydroquinone- and azide-functionalized RGD, HQ-RGD; (2) cyclic RGD-functionalized oxyamine, cRGD; (3) PHSRN-functionalized oxyamine, PHSRN; (4) KKKTTK-functionalized oxyamine, KKKTTK; (5) galactose-functionalized oxyamine, Gal; (6) mannose-functionalized oxyamine, Man; (7) alkyne-terminated tetra(ethylene glycol) alkanethiol, alkyne-EG_4SH; and (8) tetra(ethylene glycol)-terminated alkanethiol, EG_4SH.

3.38 mmol, 1.5 equiv) in H_2O (10 mL) and EtOH (5 mL). The reaction formed a cloudy orange precipitate and was stirred for 16 h at room temperature. The mixture was diluted with DCM (30 mL), extracted with H_2O (4 × 100 mL), stirred in a solution containing EDTA (2 × 50 mL, 10 mM in H_2O) for 10 min, dried over $MgSO_4$, and concentrated. The colorless oil was then purified via silica flash column chromatography using a gradient of MeOH/DCM (0−5% MeOH) to afford a white solid, **D** (1.02 g, 61.1%). HRMS (*m/z*): $[M]^+$ calcd for $C_{42}H_{50}N_4O_8$ 738.36, found 738.38. HPLC: t_r = 15.2 min, 0.1% TFA and 5−50% H_2O/ACN over 25 min.

Solid-Phase Peptide Syntheses (SPPS). Rink amide MBHA resin (0.127 g, 0.1 mmol) was delivered to an automated glass chamber for peptide synthesis. The amino acids listed above were measured (0.30 mmol) and diluted in 5 mL of DMF (10 mL for Ser and Gly) and also delivered to peptide synthesizer chambers. The following reagents were prepared in DMF: 0.1 M HBTU, 0.1 M DIEA, and 20% piperidine. The peptide synthesizer (C S Bio Co., Peptide Synthesizer Division, Menlo Park, CA) was programmed to generate the following sequences, separately, over the course of 12 h: resin-S-S-D-G-R-G-G(HQ)-C_6(linker)-K(N_3)-amide (**1**), resin-S-D-G-R-G-C_6(linker)-ONH_2 (**2**), resin-N-R-S-H-P-K-C_6(linker)-ONH_2 (**3**), and resin-K-T-T-K-K-K-C_6(linker)-ONH_2 (**4**). Following elongation, the resin was washed with DMF and DCM repeatedly and then cleaved from the resin in an N_2-bubbling solution of H_2O/TFA (10 mL, 0.25:9.75) for 1 h. The filtrate was drained into a tube containing cold ether to form a white precipitate that was then centrifuged (2 × 2000 rpm, 10 min), dissolved in H_2O (10 mL), and lyophilized (FreeZone 2.5, Labconco Corp., Kansas City, MO) overnight to afford a white solid, **1** (54 mg, 65%). HRMS (*m/z*) HQ-RGD: $[M]^{2+}$ calcd for $C_{52}H_{84}N_{19}O_{16}$ 615.32, found 616.47. HRMS (*m/z*) RGD-OA: $[M]^+$ calcd for $C_{25}H_{46}N_{11}O_{11}$ 676.34, found 676.31. HRMS (*m/z*) PHSRN-OA: $[M]^+$ calcd for $C_{38}H_{67}N_{16}O_{11}$ 923.52, found 923.56. HRMS (*m/z*) KKTTK-OA: $[M]^+$ calcd for $C_{40}H_{79}N_{13}O_{11}$ 917.59, found 917.46.

Preparation of Gold-Coated Substrates and Monolayers. Glass coverslips (75 × 25 mm^2) were immersed into a piranha solution (1:3 (v:v) concentrated H_2SO_4:30% H_2O_2; **use with caution**) for 4 h, followed by rinsing with deionized H_2O and EtOH. Gold substrates were prepared by electron-beam deposition (Model VE-100, Thermionics Laboratory, Inc., Port Townsend, WA) of titanium (5 nm) and then gold (12 nm for cell work and 50 nm for electrochemical measurements). The gold-coated slides were cut into 1 × 2 cm^2 pieces. To form SAMs on gold, the slides were immersed in an ethanolic solution containing the alkanethiols (1 mM of 5% alkyne-EG_4SH for cell studies and 100% alkyne-EG_4SH for electrochemical characterization) for at least 16 h. Once removed from solution, the surfaces were rinsed with EtOH and dried with an air stream before use.

HQ-RGD Immobilization. After monolayer formation with 1 mM of 1% alkyne-EG_4SH/EG_4SH, a solution containing 10 mmol HQ-RGD, 15 mmol $CuSO_4{\cdot}5H_2O$, and 15 mmol NaASc (1:1:1) in H_2O and EtOH (3:1) was added to the substrates and allowed to react for 90 min. Substrates were then rinsed with EtOH and dried with a stream of air, and HQ-RGD immobilization was confirmed by cyclic voltammetry (CV).

Electrochemical Activation. Electrochemical experiments were performed using a BAS 100B/W electrochemical analyzer (Bioanalytical Systems, Inc., West Lafayette, IN) in a 1 M $HClO_4$ electrolyte solution with an Ag/AgCl electrode serving as the reference, the gold monolayer as the working electrode, and a Pt wire as the counter electrode. Surfaces were scanned at a rate of 100 mV/s from −100 to 850 mV to activate "on" (quinine form).

Ligand Immobilization and Release. Peptides and sugars were added to RGD-Q-presenting surfaces (20 mM in H_2O) and allowed to react for 90 min. Immobilized ligands were confirmed using the same electrochemical parameters listed above. The ligands were released by applying potential for 12 cyclic scans (−100 to 850 mV) in PBS buffer (pH 7) and were characterized using similar conditions.

Cell Culture and Surface Seeding. Swiss albino 3T3 mouse fibroblasts were cultured in Dulbecco's modified Eagle medium containing 10% calf bovine serum and 1% penicillin/streptomycin. When passaging or seeding, a 1 mL solution of 0.05% trypsin in 0.53 mM EDTA was employed to remove cells from the tissue culture plastic. For passaging, cells (10^5 cells/mL) were then added to a new culture flask containing fresh media and placed in the incubator (37 °C, 5% CO_2) to grow and divide. For surface seeding, cells were resuspended in serum-free medium (10^5 cells/mL) and diluted to 10^3 cells/mL with serum-free medium. The cells were then seeded to surfaces for 2 h, and after 2 h, serum-containing media was added to promote cell growth.

Cell Staining. After 2 h of cell growth, the cells were fixed with formaldehyde (3.2% in PBS) and then permeated (PBS containing 0.1% Triton X-100). Two fluorescent dye mixtures were made with the following components: 10 mmol of phalloidin (1.6 μL), 10 mmol of antipaxillin or antivinculin (1 μL), and 5% normal goat serum with 0.1% Triton X -100 (397.4 μL), or 10 mmol of phalloidin (10 μL), 10 mmol of Cy-2 (1.25 μL), 1 mmol of DAPI (μL), and 5% normal goat serum with 0.1% Triton X-100 (487.8 μL). Cells were immersed in each staining solution for 1 h. The substrates were then secured with their gold-coated side down in fluorescence mounting medium (Dako, Carpinteria, CA), which enhances the visualization of cells when viewed under a fluorescent microscope, on a glass coverslip.

Fluorescence Microscopy. Fluorescent images were obtained with a Nikon Eclipse TE2000-E inverted microscope (Nikon USA, Inc., Melville, NY) and a Plan Fluor 40× oil immersion objective (1.30 NA, Nikon USA). Immersion oil was purchased from Carl Zeiss MicroImaging, Inc. (Thornwood, NY) and the lens paper was

dx.doi.org/10.1021/la503521x | *Langmuir* 2014, 30, 13656−13666

obtained from Fisher. Image analysis was performed using MetaMorph software (Molecular Devices, Downingtown, PA).

Cell Adhesion Assay. The number of adhered cells were measured 2 h after seeding on the following substrates at 2% ligand density: ±HQ-RGD and Gal, Man, PHSRN, KKKTTK, and cRGD. Two hundred microliters of cells (~10^3 cells/mL) was added to each substrate (1 cm^2), which was subsequently incubated at 37 °C and 5% CO_2 for 2 h. Two random regions of four different substrates for each ligand combination were imaged at a 4× resolution using a Nikon Eclipse TS100 (Nikon USA, Inc., Melville, NY). The attached cells were then counted. The data are expressed as the mean ± SEM of eight replicates.

Cell Area Determination Assay. Cell areas (μm^2) were measured 2 h after seeding on the following substrates at 2% ligand density: ±HQ-RGD and Gal, Man, PHSRN, KKKTTK, and cRGD. Two hundred microliters of cells (~10^3 cells/mL) was added to each substrate (1 cm^2), which was subsequently incubated at 37 °C and 5% CO_2 for 2 h. The cells were then fixed as previously reported, and two random cell areas from four different substrates for each ligand combination were imaged at a 20× resolution using a Nikon Eclipse TS100 (Nikon USA, Inc., Melville, NY). Image analyses (Nikon Eclipse TE2000-E inverted microscope; Nikon USA, Inc., Melville, NY),was carried out with MetaMorph software (Molecular Devices, Downingtown, PA). The data are expressed as the mean ± SEM of eight replicates.

Cell Migration Rate Determination. Cells were cultured and seeded at concentrations of approximately 10^3 cells/mL onto the following substrates at 2% ligand density, as described: HQ-RGD and HQ-RGD + Gal, Man, PHSRN, KKKTTK, or cRGD. Migration rates were determined after recording the movement of cells for 18 h in bright-field mode (Nikon Eclipse TE2000-E inverted microscope; Nikon USA, Inc., Melville, NY). Eight randomly selected cells (four cells per substrate condition, two substrates per condition) were imaged each hour for 18 h, and the displacements from their original adherent position were tracked and calculated using MetaMorph software (Molecular Devices, Downingtown, PA). The data are expressed as the mean ± SEM of eight replicates.

Electrochemical Characterization. HQ-RGD was immobilized to alkyne-terminated SAMs (100%, 1 mM in EtOH, 16 h), as previously described. The immobilization was confirmed using a BAS 100B/W electrochemical analyzer (Bioanalytical Systems, Inc., West Lafayette, IN) in a 1 M $HClO_4$ electrolyte solution with an Ag/AgCl electrode serving as the reference, the gold monolayer as the working electrode, and a Pt wire as the counter electrode. Samples were scanned at 100 mV/s ranging from −100 to 850 mV. To immobilize oxyamine-containing ligands, the substrates were activated and turned on after performing a linear scan from −100 to 850 mV at 100 mV/s. After ligand immobilization, the redox reversible oxime signal was confirmed using CV with the parameters just mentioned. The ligands were then release, as described, and confirmed by CV.

Enzymatic Adhesion Assay. Fbs (~10^4 cells/mL) were suspended in serum-free media and treated separately with heparinase I and heparinase II (0.025 U/mg), chondroitinase ABC (0.025 U/mg), or no enzyme (control) for 30 min at room temperature. Cells were then seeded to substrates presenting 2% HQ-RGD and 2% HQ-RGD + KKKTTK for 2 h, after which the surfaces were fixed. Two random regions of four different substrates for each ligand combination were imaged at a 4× resolution using a Nikon Eclipse TS100 (Nikon USA, Inc., Melville, NY). The attached cells were then counted. The data are expressed as the mean ± SEM of eight replicates.

Cell Detachment Assay with Soluble Molecules. Fbs (10^4 cells/mL) were seeded in a suspension of serum-free media on the following substrates at 2% ligand density for 4 h: HQ-RGD + PHSRN, KKKTTK, or cRGD. After 4 h, several soluble molecules, GRGDS, cGRDSF, HS, and FN (0.1 μM), were added for 1 h. The Fbs were then fixed. Two random regions of three to four different substrates for each ligand combination were imaged at a 4× resolution using a Nikon Eclipse TS100 (Nikon USA, Inc., Melville, NY). The attached cells were then counted. The data are expressed as the mean ± SEM of 5−8 replicates.

Focal Adhesion Kinase (FAK) Assay. Fbs (10^6 cells/mL) were incubated for 4 h on the following substrates at 2% ligand density: HQ-RGD + PHSRN, KKKTTK, or cRGD. After incubation, the FAK protein levels were detected and quantified using an ELISA kit (Invitrogen, Camarillo, CA), following the manufacturer's instructions. Briefly, the cells were removed from each substrate with trypsin, centrifuged (1000 rpm, 5 min), resuspended in ice-cold PBS (2 mL), centrifuged (1000 RMP, 5 min), and lysed. Then, 50 μL of the FAK detection antibody was added and incubated with 50 μL of each cell sample for 3 h at room temperature, after which the samples were aspirated and washed with PBS (4 × 2 mL). The samples were then incubated with 100 μL of HRP anti-rabbit antibody for 30 min at room temperature and then washed (4 × 2 mL PBS). One hundred microliters of Stabilized Chromagen was then added for 30 min at room temperature, after which 100 μL of stop solution was then added to each sample. The optical densities were measured at 450 nm using a Beckman Du-640 spectrophotometer (GMI, Ramsey, MN) and compared to the standard FAK concentrations.

RESULTS AND DISCUSSION

Dynamic Surface Design and Ligand Selection Rationale. The development and use of smart materials that have switchable or stimuli-responsive properties have proven to be important for a number of biological studies ranging from fundamental basic cell biology research to biomedical implants and tissue engineering scaffolds.[31−34] Therefore, we aimed to modulate the dynamic ECM with redox-responsive surfaces to survey ligand effects on cell behavior. FN is an abundant glycoprotein that promotes cell adhesion to the ECM via integrin (i.e., transmembrane, cell surface receptors) interactions (Figure 1A). Two key peptide sequences, Arg-Gly-Asp (**1**, RGD, Scheme 2) and Phe-His-Ser-Arg-Asn (**3**, PHRSN, Scheme 2), located in $FNIII_{10}$ and $FNIII_9$, respectively, were identified as cell-binding ligands. Polymers, nanoparticles, and other biomaterials are routinely functionalized with both linear ($K_d \sim \mu M$) and cyclic (**2**, cRGD; $K_d \sim$ nM, Scheme 2) forms of RGD to promote integrin recognition and subsequent cell attachment.[44,45] PHSRN is described as a synergy ligand with RGD and interacts simultaneously with $\alpha_5\beta_1$ integrins to mediate cell adhesion and migration.[15−18] Furthermore, an HS binding domain, located within $FNIII_{12\text{-}14}$, was identified and promotes cell surface syndecan and integrin corecognition and interaction. With the FN structure in mind, we hoped to reproduce the combined ligand effects of coupling PHSRN and cRGD with RGD on cell adhesion, spreading, morphology, and migration. As a new ligand, we chose to survey the combined effects of RGD and Lys-Lys-Lys-Thr-Thr-Lys (**4**, KKKTTK, Scheme 2), which bares four positive charges, on cell behavior. We assumed that KKKTTK would mediate electrostatic interactions with negatively charged cell surface HSPGs, mimicking the HS binding domain on FN and producing a synergistic effect on cell adhesion, growth, and migration. Detailed peptide structures are displayed in Scheme S2 in the Supporting Information.

We also chose to investigate the dual-ligand effects of RGD with galactose (**5**, Gal, Scheme 2) and mannose (**6**, Man, Scheme 2) monosaccharides due to a few published works. Du et al. reported the enhancement of hepatocyte adhesion using a hybrid Gal/RGD monolayer via hepatic asialoglycoprotein receptor interactions.[46] Fbs that express the mannose receptor, which contains a FNII domain, have been shown to exhibit specificity in binding to type I, III, and IV collagens to facilitate cell−ECM adhesion.[47] Thus, we hypothesized to observe an

dx.doi.org/10.1021/la503521x | Langmuir 2014, 30, 13656−13666

increase in cell adhesion and spreading and a decrease in migration when presented with RGD.

The general dynamic redox-responsive surface strategy to present two ECM ligands is represented in Figure 1B,C, and a more detailed schematic is provided in Scheme S1 (Supporting Information (SI)). Mixed EG_4SH/alkyne-EG_4SH SAMs (Scheme 2) were formed on gold substrates in a ratio of 99:1 (1 mM total in EtOH, 16 h). Both alkanethiols are resistant to nonspecific protein adsorption and cell adhesion, which is extremely important when conducting biospecific ligand−receptor interaction studies.[48−50] Here, EG_4SH (99% density) serves as the inert background and alkyne-EG_4SH (1% density) provides an alkyne terminal group for ligand immobilization via click chemistry with an azide-containing RGD ligand. The molecule density was maintained at 1% to ensure that only the specific interactions between the ligands in question with Fb cell surface receptors occur.

The redox-responsive trigger, in the form of a hydroquinone/quinone (HQ/Q) couple, was built into an Fmoc-protected glycine residue (**E**, Scheme 1A) and was compatible with routine solid-phase peptide synthesis (Figure S1, SI). **E** was incorporated into an RGD-containing peptide (**1**, HQ-RGD, Schemes 1 and 2) that was capped with an azide-functionalized lysine residue for coupling to the 1% alkyne-EG_4SH SAMs via click chemistry (20 mM in H_2O/EtOH (3:1), cat. $CuSO_4 \cdot 5H_2O$ and NaAsc, 90 min). We have previously shown and extensively characterized the immobilization and release of oxyamine (OA)-functionalized ligands (i.e., peptides, small molecules, and carbohydrates) to and from HQ/Q SAMs on gold substrates for a number of biotechnological applications and cell behavioral studies.[37−39] As shown in Figure 1B, after HQ-RGD-N_3 immobilization to alkyne-EG_4SH SAMs, the substrates are oxidized [Ox] using linear sweep voltammetry to the corresponding Q (1 M $HClO_4$, −100 to 850 mV, 100 mV/s), which then reacts rapidly and chemoselectively at room temperature and under physiological conditions (20 mM in PBS, pH of 7, 2 h) to form an oxime conjugate. The oxime bond is stable in all pH ranges until application of a reducing potential at a pH of 7, at which the ligands are spontaneously cleaved, regenerating the original HQ-RGD-tethered SAM.[38,39] Ligand immobilization and release to and from HQ-RGD-presenting SAMs were characterized by electrochemistry and fluorescence microscopy (Figures S2 and S3, respectively, SI). A key feature of this system is that both HQ-RGD and the corresponding oxime conjugate exhibit signature redox signals that can be monitored and quantified by cyclic voltammetry (CV) in terms of ligand immobilization, release, and density, characteristics that are significant when designing a platform for biological investigation. Thus, this dual-ligand ECM and combinatorial screening strategy possesses the following features: a dynamic, molecular redox-responsive trigger for immobilizing and releasing structurally well-defined ligands in the presence of cells; density control over ligands; and rapid, chemoselective, and bioorthogonal coupling reactions (i.e., Huisgen cycloaddition and oxime chemistry).

Cell Adhesion Assays. Before testing our dual-ligand ECM system, we first verified whether Fbs could adhere and healthily spread on substrates presenting HQ-RGD and each decoupled ligand (Figure 2). As such, HQ-RGD and cRGD, Man, Gal, PHSRN, and KKKTTK ligands were immobilized to alkyne-EG_4SH (20 mM in H_2O/EtOH (3:1), cat $CuSO_4 \cdot 5H_2O$ and NaAsc, 90 min) and HQ-terminated (20 mM in PBS, 2 h) SAMs, respectively, at a 2% ligand density. Fbs cells were then

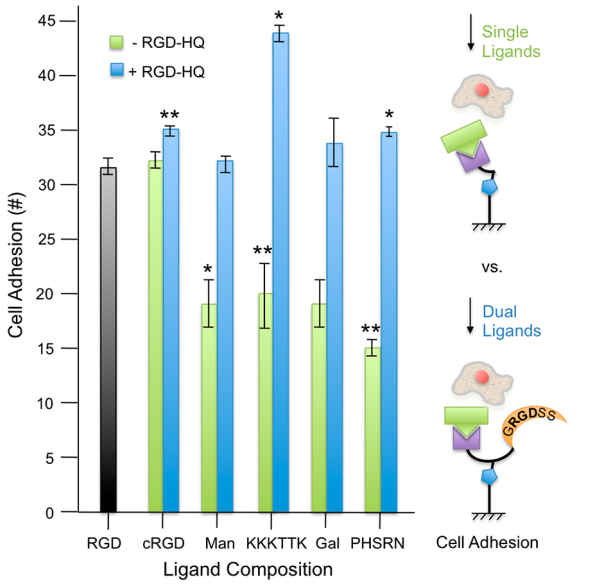

Figure 2. Number of adhered cells after 2 h of culture on the following substrates: single ligands (green) cRGD, Man, KKKTTK, Gal, or PHSRN; dual ligands (blue) HQ-RGD + cRGD, Man, KKKTTK, Gal, or PHSRN. Statistical analyses were performed with respect to HQ-RGD: $*p < 0.001$ and $**p < 0.01$.

seeded to surfaces (~10^3 cells/mL, 2 h), fixed, imaged, and counted after 2 h. As shown in Figure 2, all ligands were able to support cell adhesion to varying degrees. The data are represented as the average number of attached cells per 4× frame (eight random regions). HQ-RGD and cRGD demonstrated similar affinity for attracting Fbs when compared to the surfaces presenting Man, Gal, KKKTTK, and PHSRN, which exhibited almost a 2-fold reduction in the amount of attached Fbs. Additionally, the Fbs were more loosely adhered and adopted a rounder morphology on substrates presenting Man, Gal, KKKTTK, and PHSRN. However, when these ligands were combined with and immobilized to SAMs with 1% Q-RGD (2% ligand total), the amount of cells increased significantly, approximately 2-fold, resembling the results observed with 2% HQ-RGD. When Man and Gal were coupled to HQ-RGD, Fbs behaved similarly to when in the presence of cell adhesive RGD; similar numbers of attached cells and mor phologies were observed. When PHSRN was coupled to HQ-RGD, a synergistic effect on the amount of cells adhered and over cell spreading and morphology was observed, although, at surface value, the actual number of attached cells did not increase significantly from the substrates with 2% HQ-RGD. Surprisingly, KKKTTK coupled to HQ-RGD showed a dramatic increase in the amount of attached Fbs when compared to HQ-RGD- and KKKTTK-presenting substrates, indicating a profound synergistic effect between KKKTTK and RGD on adhesion. A marked 0.5-fold increase from HQ-RGD substrates was observed on KKKTTK + HQ-RGD.

Cell Spreading, Morphology, and Migration Assays. Upon adhering to the ECM or another cell, a cell undergoes the following sequential events: spreading, actin cytoskeleton organization, and focal adhesion (FA) formation (Figure 1A). The cell then waits in anticipation of receiving and processing extracellular signals and migrates from various epithelial layers to target locations, where it differentiates to form a specialized cell that comprises different tissues and organs.

dx.doi.org/10.1021/la503521x | *Langmuir* 2014, 30, 13656−13666

Similar immobilization and fixing conditions were employed to survey the possible synergistic or antagonistic effects of coupling cell adhesive RGD with a number of peptides and carbohydrates on cell spreading, morphology, and migration rate. Cell areas were measured, and FAs and actin were visualized by staining for vinculin (antivinculin and Cy-2, green) and F-actin (phalloidin, red) after 2 h of culture on all surfaces (Figure 3A,B). Cells were then observed to migrate on substrates during an 18-h period via life-cell recordings, and migration rates were calculated (Figure 3C). Notably, the focus of this work was to observe the possible synergistic or antagonist effects of an artificial, dual-ligand ECM. Our cell attachment and spreading results in Figures 2 and 3A, respectively, demonstrate significant increases in the size and number of cells adhered to dual-ligand-presenting SAMs when compared to substrates displaying single HQ-RGD, cRGD, PHSRN, KKKTTK, Gal, and Man ligands. Thus, cell migration behavior was only examined on dual-ligand surfaces.

As shown in Figure 3A,B, when compared to HQ-RGD, Fbs were extremely well spread on both cRGD and HQ-RGD + cRGD presenting surfaces. These results are not surprising, because the RGD sequence in native FN is located on a β-turn, and thus, the cyclic form of RGD has a nanomolar affinity for integrin binding, compared to linear RGD, which has micromolar cell-binding affinity.[51,52] Cells exhibited a 30% increase (HQ-RGD, 630 μm^2; cRGD, 850 μm^2; HQ-RGD + cRGD, 850 μm^2) in area from HQ-RGD with a more pronounced and intricate network of actin striations and FAs on the periphery and along the actin extensions of the main cell body (right panel, Figure 3B). These morphological characteristics are indicative of well-adhered, healthy cells. Moreover, when comparing Fb migration on HQ-RGD (7.2 $\mu m/h$), cells exhibited a 2-fold decreased rate (3.1 $\mu m/h$) on HQ-RGD + cRGD, corroborating the adhesion, spreading, and morphology data (Figure 3C).

Synergistic effects of coupling HQ-RGD + PHSRN on Fb spreading and morphology were observed, verifying the results from the cell adhesion assay. An approximate 4-fold increase in average cell area from PHSRN (180 μm^2) to HQ-RGD + PHSRN (700 μm^2) was recorded, indicating that PHSRN, which resembles $FNIII_9$, does not alone sustain adequate attachment and growth. This result was expected due to the lower binding affinity of integrins for PHSRN.[18,30] Moreover, cells were larger on average than those on HQ-RGD alone (630 μm^2). The cell morphologies were drastically different upon observing Figure 3A,B. Cells on PHSRN alone remained small with rounded ruffling features at the cell periphery and little to no FA formations, as compared to cells on HQ-RGD. However, when coupled to HQ-RGD, cells spread but appeared to be in a migratory state; the actin cytoskeleton was not fully extended and striated and FAs were not strongly pronounced. These cellular characteristics were further verified with the migration data represented in Figure 3C. Cells on HQ-RGD + PHSRN (11.9 $\mu m/h$), demonstrated a 66% increase in migration rate when compared to cells on HQ-RGD (7.2 $\mu m/h$). These results demonstrate a relationship between increased migration rate and cell ruffling dynamics, suggesting that our cell findings on RGD/PHSRN substrates were induced by ligand effects. These data corroborate previous reports showing that PHSRN causes ECM invasion of Fbs and keratinocytes and stimulates corneal epithelial cell migration, accelerating wound healing in mice and rabbits, respectively.[53,54]

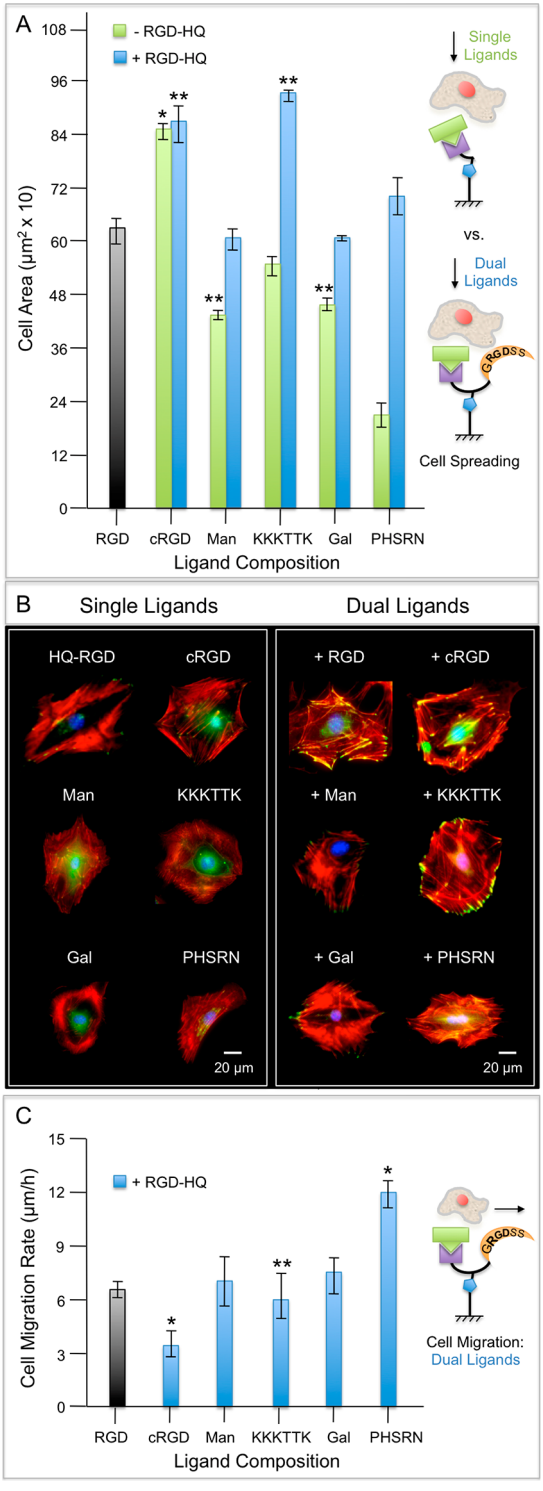

Figure 3. Representative cell areas (A), morphologies (B), and migration rates (C) after 2 h of culture on the following substrates presenting single ligands (green) cRGD, Man, KKKTTK, Gal, or PHSRN and dual ligands HQ-RGD (blue) + cRGD, Man, KKKTTK, Gal, or PHSRN. Cells in part B were stained for actin (red, phalloidin), nucleus (blue, DAPI), focal adhesions (FAs, green, antivinculin/Cy 2). Migration rates were calculated from an 18-h period using live-cell recording and imaging software. Each bar represents the mean ± SEM (n = 8). Statistical analyses were performed with respect to HQ-RGD: *p < 0.001 and **p < 0.01.

dx.doi.org/10.1021/la503521x | Langmuir 2014, 30, 13656−13666

Although marked differences were observed in the Fb spreading, areas, and morphologies on Gal and HQ-RGD + Gal (420−600 μm^2) and Man and HQ-RGD + Man (380−610 μm^2), no overall synergistic effects were observed when compared to HQ-RGD alone (630 μm^2) (Figure 3A). This conclusion was also apparent from the images in Figure 3B. Similar to PHSRN, Fbs on Gal and Man adopted small and round shapes with no noticeable FA formations and organized actin cytoskeleton. Ruffling characteristics are typical of cells that are feeling and sensing their environment. The increase in cell area after Man and Gal immobilization to Q-RGD is most likely due to the presence of cell adhesive RGD. The cells appear more spread with FA formations at the tips of spikey actin extensions. However, the cell bodies remain rounded, and the actin cytoskeleton is not well structured; it appears that these monosaccharide ligands may be partially masking the adhesive properties of RGD. When observing the migration data, the rate differences were minimal when comparing cells on HQ-RGD and HQ-RGD + Man or Gal substrates (7.2, 7.4, and 7.5 $\mu m/h$, respectively). Interestingly, Fbs migrated at approximately the same rate on both RGD and carbohydrate-presenting SAMs (Figure 3C).

As previously mentioned, KKKTTK weakly supported the attachment of Fbs. However, when compared to the average area of cells on HQ-RGD (630 μm^2), cells on KKKTTK alone exhibited a comparable average area of 560 μm^2. Although no defined FAs were formed on the cell peripheries (left panel, Figure 3B), the actin cytoskeleton appeared to be partially organized, with striated patterns and small extensions. This area may be due to the electrostatic interactions, generated from the positive lysine residues at physiological conditions and highly negatively charged cell surface. When coupled to HQ-RGD, the average cell area on KKKTTK + HQ-RGD increased by approximately 50% that of cells on HQ-RGD alone, indicating a synergistic effect of spreading and growth. When imaged, cells maintained a rounded, spread, dense cell body, as seen with cells on KKKTTK alone; however, the appearance of strongly pronounced FAs at the cell periphery and increased actin organization was observed (left panel, Figure 3B). When considering the difference in cell migration rates, Fbs on HQ-RGD + KKKTTK demonstrated a 20% decrease from that of cells on HQ-RGD alone. The data was statistically significant ($p < 0.0001$), indicating that the presence of KKKTTK does exhibit a combined ligand effect. These significant morphological distinctions and decreased migration rate further support the synergistic effects of RGD ($FNIII_{10}$) and KKKTTK ($FNIII_{12-14}$) in promoting cell surface integrin and syndecan interactions.

Ligand Inhibition Studies on Cell Adhesion. Because the ligand combinations HQ-RGD + cRGD, HQ-RGD + KKKTTK, and HQ-RGD + PHSRN demonstrated an effect on Fb adhesion, several soluble molecule and enzyme inhibition studies were performed. We first surveyed the number of attached cells on HQ-RGD + cRGD, HQ-RGD + KKKTTK, and HQ-RGD + PHSRN substrates (2%) before and after the addition of FN, cRGD, and HS (0.1 mmol in PBS). FN is a natural adhesion protein in the ECM, and we choose cRGD because integrins have a high binding (nM) affinity for the ligand. HS is a repeating disaccharide that possesses a carboxylate and varying sulfate groups. Thus, at physiological conditions, the overall net charge of HS is highly negative. We assumed that addition of soluble FN, cRGD, and HS would interfere with the binding interactions of Fbs and our dual-ligand ECM substrates. In Figure 4A, the addition of soluble FN had significant effects on the cells that were adhered to HQ-

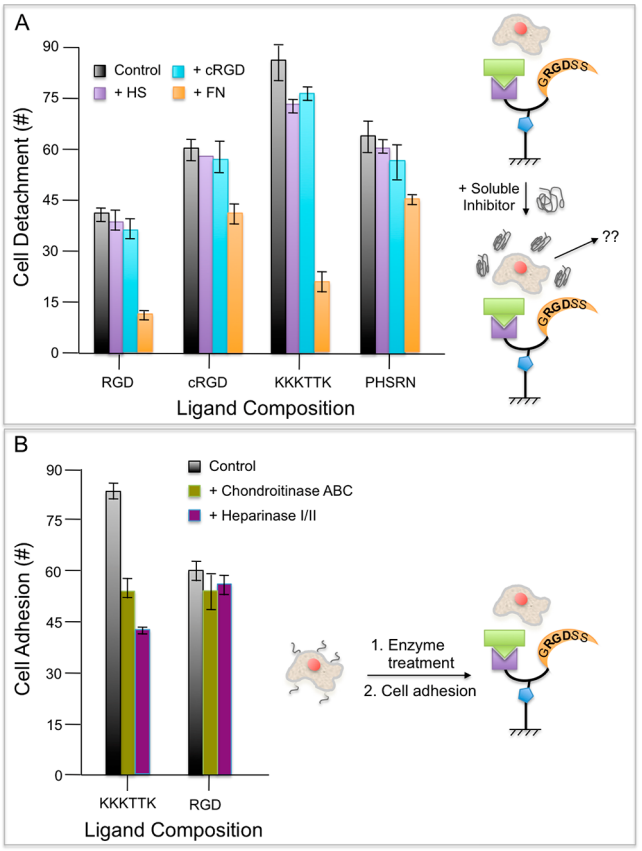

Figure 4. Cell adhesion inhibition assays. (A) Soluble competitive inhibition studies with (orange) FN, (blue) cRGD, and (light purple) HS and (B) enzymatic treatment of cells with (olive green) chondroitinase ABC and (dark purple) heparinase I/II on the following substrates: HQ-RGD and HQ-RGD + cRGD, KKKTTK, or PHSRN. Each bar (mean ± SEM) represents an average of five to eight trials (~10^4 cells/mL).

RGD and HQ-RGD + KKKTTK; an approximate 75% reduction of attached cells was observed. Thirty percent of the Fbs on HQ-RGD + cRGD detached from the surface after FN addition, and only 10% lifted from HQ-RGD + PHRSN, as expected. Therefore, RGD alone and the combination of RGD with KKKTTK or cRGD do not exhibit as strong of a synergistic effect on promoting strong cell attachment as originally anticipated. For all substrates, the addition of soluble cRGD and HS had minimal effects on Fb detachment. The high binding affinity small peptide and negatively charge oligosaccharide were not strong enough to detach the cells from the dual-ligand ECM mimics, most likely due to already established cell surface integrin− and syndecan−ligand interactions. On the basis of the other evidence in this section, RGD + KKKTTK remains a good dual-ligand ECM platform, but is not as ideal as natural ligand FN.

We also investigated the enzymatic effects of heparinase I and II (Hep I/II) and chondroitinase ABC (chon ABC) on cleaving the HS and CS chains of PGs that are found on Fb membranes. These enzymes were incubated with Fbs at 0.025 units/mg in serum-free media for 1 h, after which the cells were added to HQ-RGD and HQ-RGD + KKKTTK (2%) for 2 h. The Fbs were then fixed, counted, and compared to the

dx.doi.org/10.1021/la503521x | Langmuir 2014, 30, 13656−13666

controls (−Hep I/II or −Chon ABC). Figure 4B presents the number of adhered cells after enzyme treatment. As shown, HQ-RGD showed little change in attracting cells to the surface with the following results: no treatment, 59; +Hep I/II, 57; and +chon ABC, 55. This could be due to the fact that only a net charge of +1 is present in the same ligand area (arginine in HQ-RGD). Therefore, cleaving the HS and CS groups from cell surfaces did not have an effect on integrin-mediated cell attachment. However, when compared to HQ-RGD + KKKTTK, Fbs experienced a 50% decrease in adhesion after enzymatic treatment of Hep I/II and chon ABC with the following results: no treatment, 83; +Hep I/II, 41; +chon ABC, 53. Furthermore, the results corroborated the previous adhesion results; more cells adhered to surfaces due to the synergistic effects of HQ-RGD and KKKTTK. The inhibition in cell adhesion after Hep I/II and chon ABC treatment is most likely due to the decreased electrostatic interactions of the negatively charged cell surface with positively charged dual-ligand ECM (+5 net charge in one concentrated area), as well as less interaction with syndecan-4 surface receptors.

Focal Adhesion Kinase Assay. To confirm the results from inhibition and morphological assays, we detected and quantified the FAK levels in cells subject to HQ-RGD + cRGD, HQ-RGD + KKKTTK, and HQ-RGD + PHSRN substrates. FAK serves a major role in cell adhesion, spreading, differentiation, migration, division, and apoptosis. Evidence of enhanced FAC was observed in morphological data of the dual-ligand ECM systems listed above. Thus, Fbs were incubated on these substrates for 4 h, and using an ELISA kit and spectrophotometry, the FAK levels were quantified. The lysates of each cell population were diluted to measure the FAK level range and generate a linear relationship between the optical density and FAK concentration. The total FAK concentration was then determined according to each substrate. As shown in Figure 5, higher FAK concentrations were observed in Fbs after

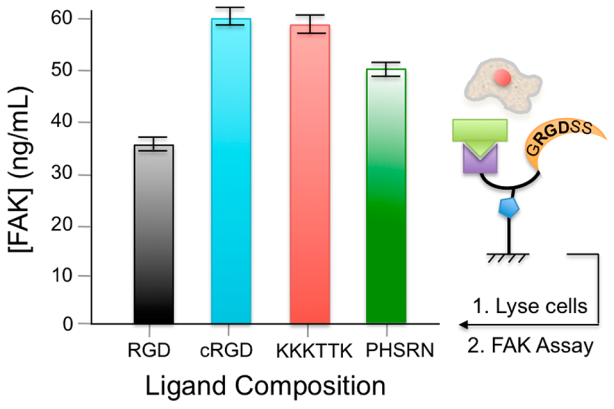

Figure 5. Total FAK (ng/mL) concentrations measured in cells on the following substrates: (black) HQ-RGD and HQ-RGD + (blue) cRGD, (pink) KKKTTK, or (green) PHSRN. Each bar (mean ± S.E.M.) represents an average of three trials from the same batch dilution (~10^6 cells/mL).

ligand immobilization to HQ-RGD SAMs when compared to substrates only baring HQ-RGD (35 ng/mL, black), with +cRGD (59 ng/mL, red) and +KKKTTK (58 ng/mL, blue) surfaces possessing similar FAK levels, followed by +PHSRN (50 ng/mL, green) functionalized substrates. Therefore, the FAK assay confirmed the morphological data; more FAs were formed in the cells on +KKKTTK and +cRGD and less in the cells on +PHSRN when compared to HQ-RGD. The combined ligand effects of RGD with KKKTTK on enhancing cell adhesion and FA formation, as determined by the increased FAK concentration, were again verified. Thus, RGD + KKKTTK is a good dual-ligand ECM mimic.

Modulation of Cell Behavior via a Dynamic ECM Model Surface. The final study in this work concerned the dynamic release of immobilized ligands in the presence of cells. Fb spreading areas, migration rates, and morphologies were investigated after releasing PHSRN, Gal, Man, KKKTTK, and cRGD from separate HQ-RGD-presenting SAMs. The data are presented in Figure 6A−C. Remarkably, after ligand release and

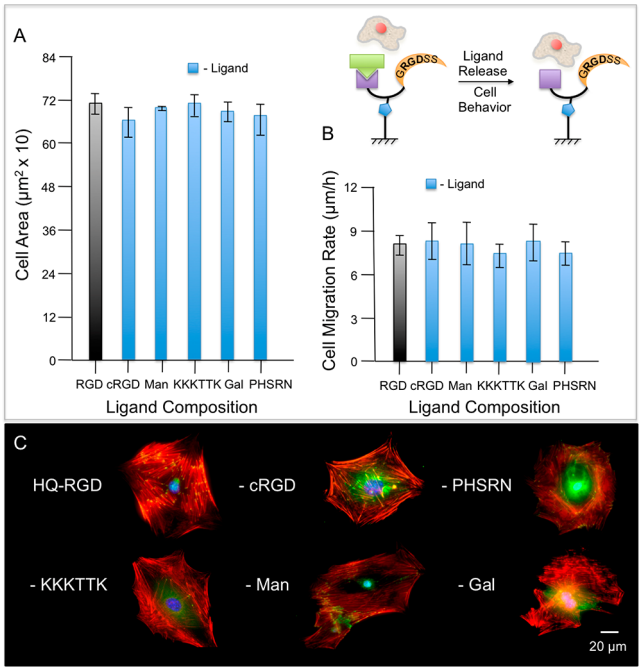

Figure 6. Cell behavioral responses to the dynamic release of ECM ligands. Cell (A) areas, (B) migration rates, and (C) morphologies after releasing (blue) cRGD, Man, KKKTTK, Gal, or PHSRN from HQ-RGD. Fbs were cultured on the dual ECM ligand-presenting surfaces for 2 h, after which the ECM ligands were electrochemically released (PBS, pH 7, 12 cyclic scans: −100 to 850 mV, 100 mV/s) and incubated for an additional 2 h. Migration rates were calculated from an 18-h period using live-cell recording and imaging software after ligand release. Each bar (mean ± SEM) represents an average of eight trials (10^3 cells/mL).

4 h adjusted time, the cells more or less adopted similar phenotypes (Figure 6C), motility (Figure 6B), and spreading areas (Figure 6A) to those of substrates that presented HQ-RGD. The Fbs that were subject to Man, Gal, and PHSRN release reorganized and extended their actin protrusions, spreading out to adopt similar sizes and migration rates. Similarly, the cells adhered to substrates in which KKKTTK and cRGD were released reorganized their actin cytoskeleton, focal adhesion assemblies, and stress fibers and contracted slightly to adapt to their new ligand stimulus, HQ-RGD. Thus, these results demonstrate the powerful nature of this surface platform in modulating the dynamic ECM environment, where ligands, proteins, and small molecules are constantly being hidden and revealed to cells.

dx.doi.org/10.1021/la503521x | Langmuir 2014, 30, 13656−13666

CONCLUSIONS

In summary, we developed a model substrate for in situ cell biological studies that dynamically modulates the ECM. A small library of biomolecules, Gal, Man, PHSRN, cRGD, and KKKTTK, was synthesized to bear an oxyamine group that reacts rapidly and chemoselectively with carbonyl moieties. This reaction is also bioorthogonal and can be performed in the presence of cells without inducing any side reactions with proteins and lipids. A cell adhesive HQ-containing RGD was also synthesized and immobilized to bioinert alkyne-EG_4SH SAMs to provide the ketone (in the form of electrochemically oxidized quinone) for dual-ligand display, and cell adhesion, spreading and growth, migration, and adhesion inhibition were measured. An added benefit of this platform included the redox-responsive trigger that turns the system on and off. Such a feature allows modulation of the dynamic ECM environment, where ligands, proteins, and small molecules are constantly being hidden and revealed to cells. In surveying the synergistic or antagonistic effects of the immobilized and released ligands to and from HQ-RGD, many key results were observed. When comparing the ligands, the number of attached cells increased for all ligands when immobilized to HQ-RGD. However, HQ-RGD + KKKTTK showed a dramatic increase of 50%, indicating a possible synergistic effect of simultaneous cell surface integrin and syndecan-4 interactions with the cell- and HS-binding domain mimics of FN. Furthermore, the formation of more FA in the morphological data was observed in the images and confirmed by the increased FAK levels from control substrates (HQ-RGD). The decreased migration rates and soluble and enzymatic inhibition assays also demonstrated that KKKTTK serves as a synergistic ECM ligand with RGD in promoting cell attachment, spreading, and division. When cRGD and PHSRN were investigated, results similar to those reported previously in the literature were observed, and Man and Gal had no effect on cell adhesion, spreading, and migration. Thus, not only does this dynamic dual-ligand ECM enable the immobilization and release of ligands in the presence of cells, but it also provides a platform for the combinatorial screening of ligands to further probe the synergistic or antagonistic effects of cell adhesive RGD with other molecules. This surface strategy can be applied to nanoparticles for the redox-state-dependent delivery and release of therapeutics and imaging probes in vitro.[39,55−58] Finally, the ability to generate defined dynamic and gradient surfaces will allow for many fundamental studies of cell behavior and for their use as biotechnology tools to assay various cell functions.[57−60]

ASSOCIATED CONTENT

Supporting Information

Detailed peptide structures, MS and HPLC characterization of HQ-containing Fmoc-gylcine, and electrochemical and fluorescent characterization of the immobilization and release of ligands to and from HQ-RGD-presenting SAMs. This material is available free of charge via the Internet at http://pubs.acs.org.

AUTHOR INFORMATION

Corresponding Author

*E-mail: chrchem@yorku.ca. Tel: (416) 736-2100, ext 77718.

Notes

The authors declare no competing financial interest.

ACKNOWLEDGMENTS

This work was supported by the Carolina Center for Cancer Nanotechnology Excellence, the Burroughs Wellcome Foundation (Interface Career Award), the National Science Foundation (Career Award), National Science and Engineering Research Council of Canada (NSERC), and the Canadian Foundation for Innovation (CFI). The authors thank J. Park for HPLC help, Brian Matthew for HPLC and MS assistance, and Nathan Westcott for valued advice.

ABBREVIATIONS USED

Alkyne-EG_4SH, alkyne-terminated tetra(ethylene glycol) alkanethiol; ECM, extracellular matrix; EG_4SH, tetra(ethylene glycol) alkanethiol; FA, focal adhesion; Fbs, fibroblasts; FN, fibronectin; cRGD, cyclic Arg-Gly-Asp; Gal, galactose; HQ, hydroquinone; HQ-RGD, hydroquinone Arg-Gly-Asp; K_d, dissociation constant; KKKTTK, Lys-Lys-Lys-Thr-Thr-Lys; Man, mannose; OA, oxyamine; Q, quinone; PHSRN, Phe-His-Ser-Arg-Asn; SAMs, self-assembled monolayers.

REFERENCES

(1) Alberts, B.; Johnson, A.; Lewis, J.; Raff, M.; Roberts, K.; Walter, P. *Molecular Biology of the Cell*; Garland Science: New York,2002.
(2) Rhodes, J.; Simons, M. The extracellular matrix and blood vessel formation: Not just a scaffold. *J. Cell Mol. Med.* **2007**, *11*, 176−205.
(3) Danilov, Y.; Juliano, R. (Arg-Gly-Asp)n−albumin conjugates as a model substratum for integrin-mediated cell adhesion. *Exp. Cell Res.* **1989**, *182*, 186−196.
(4) Williams, C. M.; Engler, A. J.; Slone, R. D.; Galante, L. L.; Schwarzbauer, J. E. Fibronectin expression modulates mammary epithelial cell proliferation during acinar differentiation. *Cancer Res.* **2008**, *68*, 3185−3192.
(5) Hood, J.; Cheresh, D. A. Role of integrins in cell invasion and migration. *Nat. Rev. Cancer* **2002**, *2*, 91−100.
(6) Bogenrieder, T.; Herlyn, M. Axis of evil: Molecular mechanisms of cancer metastasis. *Oncogene* **2003**, *22*, 6524−6536.
(7) Liotta, L.; Kohn, E. The microenvironment of the tumour-host interface. *Nature* **2001**, *411*, 375−379.
(8) Hynes, R. Integrins: A family of cell surface receptors. *Cell* **1987**, *48*, 549−554.
(9) Tamkun, J.; DeSimone, D.; Fonda, D.; Patel, R.; Buck, C.; Horwitz, A.; Hynes, R. Structure of integrin, a glycoprotein involved in the transmembrane linkage between fibronectin and actin. *Cell* **1986**, *46*, 271−282.
(10) Juliano, R.; Reddig, P.; Alahari, S.; Edin, M.; Howe, A.; Aplin, A. Integrin regulation of cell signalling and motility. *Biochem. Soc. Trans.* **2004**, *32*, 443−446.
(11) Ginsberg, M. H.; Partridge, A.; Chattil, S. J. Integrin regulation. *Curr. Opin. Cell Biol.* **2005**, *17*, 509−516.
(12) Hynes, R. Molecular biology of fibronectin. *Annu. Rev. Cell Biol.* **1985**, *1*, 67−90.
(13) Pankov, R.; Yamada, K. M. Fibronectin at a glance. *J. Cell Sci.* **2002**, *115*, 3861−3863.
(14) Pierschbacher, M. D.; Ruoslahti, E. Cell attachment activity of fibronectin can be duplicated by small synthetic fragments of the molecule. *Nature* **1984**, *309*, 30−33.
(15) Aota, S.; Nomizu, M.; Yamada, K. M. The short amino acid sequence Pro-His-Ser-Arg-Asn in human fibronectin enhances cell-adhesive function. *J. Biol. Chem.* **1994**, *269*, 24756−24761.
(16) Bowditch, R. D.; Hariharan, M.; Tominna, E. F.; Smith, J. W.; Yamada, K. M.; Getzoff, E. D.; Ginsberg, M. H. Identification of a novel integrin binding site in fibronectin. Differential utilization by beta 3 integrins. *J. Biol. Chem.* **1994**, *269*, 10856−10863.
(17) Garcia, A. J.; Schwarzbauer, J. E.; Boettiger, D. Distinct activation states of alpha 5 beta 1 integrin show differential binding to

RGD and synergy domains of fibronectin. *Biochemistry* **2002**, *41*, 9063−9069.
(18) Feng, Y.; Mrksich, M. The synergy peptide PHSRN and the adhesion peptide RGD mediate cell adhesion through a common mechanism. *Biochemistry* **2004**, *43*, 15811−15821.
(19) Leahy, D. J.; Aukhil, I.; Erickson, H. P. 2.0 Angstrom crystal structure of a four-domain segment of human fibronectin encompassing the RGD loop and synergy region. *Cell* **1996**, *84*, 155−164.
(20) Ingham, K. C.; Brew, S. A.; Atha, D. H. Interaction of heparin with fibronectin and isolated fibronectin domains. *Biochem. J.* **1990**, *272*, 605−611.
(21) Kim, J. H.; Park, S. O.; Jang, H. J.; Jang, J. H. Importance of the heparin-binding domain of fibronectin for enhancing cell adhesion activity of the recombinant fibronectin. *Biotechnol. Lett.* **2006**, *28*, 1409−1413.
(22) Lebaron, R. G.; Athanasiou, K. A. Extracellular matrix cell adhesion peptides: Functional applications in orthopedic materials. *Tissue Eng.* **2000**, *6*, 85−103.
(23) Dee, K. C.; Anderson, T. T.; Bizios, R. Design and function of novel osteoblast-adhesive peptides for chemical modification of biomaterials. *J. Biomed. Mater. Res.* **1998**, *40*, 371−377.
(24) McCarthy, J. B.; Skubitz, A. P.; Qi, Z.; Yi, X. Y.; Mickelson, D. J.; Klein, D. J.; Furcht, L. T. RGD-independent cell adhesion to the carboxy-terminal heparin-binding fragment of fibronectin involves heparin-dependent and -independent activities. *J. Cell Biol.* **1990**, *110*, 777−787.
(25) Kritz, A. B.; et al. Adenovirus 5 fibers mutated at the putative HSPG-binding site show restricted retargeting with targeting peptides in the HI loop. *Mol. Ther.* **2007**, *15*, 741−749.
(26) Darr, S.; Madisch, I.; Hofmayer, S.; Rehren, F.; Heim, A. Phylogeny and primary structure analysis of fiber shafts of all human adenovirus types for rational design of adenoviral gene-therapy vectors. *J. Gen. Virol.* **2009**, *90*, 2849−2854.
(27) Di Paolo, N. C.; Kalyuzhniy, O.; Shayakhmetov, D. M. Fiber shaft-chimeric adenovirus vectors lacking the KKTK motif efficiently infect liver cells in vivo. *J. Virol.* **2007**, *81*, 12249−12259.
(28) Buck, C. A.; Horwitz, A. F. Cell surface receptors for extracellular matrix molecules. *Annu. Rev. Cell Biol.* **1987**, *3*, 179−205.
(29) Humphries, J. D.; Byron, A.; Humphries, M. J. Integrin ligands at a glance. *J. Cell Sci.* **2006**, *119*, 3901−3903.
(30) Eisenberg, J. L.; Piper, J. L.; Mrksich, M. Using self-assembled monolayers to model cell adhesion to the 9th and 10th type III domains of fibronectin. *Langmuir* **2009**, *25*, 13942−13951.
(31) Nakanishi, J. Switchable substrates for analyzing and engineering cell functions. *Chem.—Asian J.* **2014**, *9*, 406−417.
(32) Mendes, P. M. Stimuli-responsive surfaces for bio-applications. *Chem. Soc. Rev.* **2008**, *37*, 2512−2529.
(33) Wischerhoff, E.; Badi, N.; Lutz, J.-F.; Laschewsky, A. Smart bioactive surfaces. *Soft Matter* **2010**, *6*, 705−713.
(34) Luo, W.; Yousaf, M. N. Tissue morphing control on dynamic gradient surfaces. *J. Am. Chem. Soc.* **2011**, *133*, 10780−10783.
(35) Liu, D.; Xie, Y.; Shao, H.; Jiang, X. Using azobenzene-embedded self-assembled monolayers to photochemically control cell adhesion reversibly. *Angew. Chem., Int. Ed.* **2009**, *48*, 4406−4408.
(36) Lee, E.-J.; Chan, E. W. L.; Yousaf, M. N. Spatio-temporal control of cell coculture interactions on surfaces. *ChemBioChem.* **2009**, *10*, 1648−1653.
(37) Lamb, B. M.; Yousaf, M. N. Redox switchable surface for controlling peptide structure. *J. Am. Chem. Soc.* **2011**, *133*, 8870−8873.
(38) Chan, E. W. L.; Park, S.; Yousaf, M. N. An electroactive catalytic dynamic substrate that immobilizes and releases patterned ligands, proteins, and cells. *Angew. Chem, Int. Ed.* **2008**, *47*, 6267−6271.
(39) Pulsipher, A.; Dutta, D.; Luo, W.; Yousaf, M.N. Cell surface engineering by a conjugation and release approach based on the formation and cleavage of oxime linkages upon mild electrochemical oxidation and reduction. *Angew. Chem., Int. Ed.* **2014**, *53*, 9487−9492.
(40) Li, J.; Thiara, P. S.; Mrksich, M. Rapid evaluation and screening of interfacial reactions on self-assembled monolayers. *Langmuir* **2007**, *23*, 11826−11835.
(41) Palegrosdemange, C.; Simon, E. S.; Prime, K. L.; Whitesides, G. M. Formation of self-assembled monolayers by chemisorption of derivatives of oligo(ethylene glycol) of structure HS-$(CH_2)_{11}(OCH_2CH_2)$Meta-OH on gold. *J. Am. Chem. Soc.* **1991**, *113*, 12−20.
(42) Chan, E. W. L.; Yousaf, M. N. Immobilization of ligands with precise control of density to electroactive surfaces. *J. Am. Chem. Soc.* **2006**, *128*, 15542−15546.
(43) Pulsipher, A.; Yousaf, M. N. A renewable, chemoselective, and quantitative ligand density microarray for the study of biospecific interactions. *Chem. Commun.* **2011**, *47*, 523−525.
(44) Mrksich, M. Using self-assembled monolayers to model the extracellular matrix. *Acta Biomater.* **2009**, *5*, 832−841.
(45) Lu, J.; Shi, M.; Shoichet, M. S. Click chemistry functionalized polymeric nanoparticles target corneal epithelial cells through RGD-cell surface receptors. *Bioconjugate Chem.* **2009**, *20*, 87−94.
(46) Du, Y.; Chia, S. M.; Han, R.; Chang, S.; Tang, H.; Yu, H. 3D hepatocyte monolayer on hybrid RGD/galactose substratum. *Biomaterials* **2006**, *27*, 5669−5680.
(47) Napper, C. E.; Drickamer, K.; Taylor, M. E. Collagen binding by the mannose receptor mediated through the fibronectin type 11 domain. *Biochem. J.* **2006**, *395*, 579−586.
(48) Luo, W.; Chan, E. W. L.; Yousaf, M. N. Tailored electroactive and quantitative ligand density microarrays applied to stem cell differentiation. *J. Am. Chem. Soc.* **2010**, *132*, 2614−2621.
(49) Dutta, D.; Pulsipher, A.; Luo, W.; Mak, H.; Yousaf, M. N. Engineering cell surfaces via liposome fusion. *Bioconjugate Chem.* **2011**, *22*, 2423−2433.
(50) Dutta, D.; Pulsipher, A.; Luo, W.; Yousaf, M. N. Synthetic chemoselective rewiring of cell surfaces: Generation of three-dimensional tissue structures. *J. Am. Chem. Soc.* **2011**, *133*, 8704−8713.
(51) Ostuni, E.; Chapman, R. C.; Liang, M. N.; Meluleni, G.; Pier, G.; Ingber, D. E.; Whitesides, G. M. Self-assembled monolayers that resist the adsorption of proteins and the adhesion of bacterial and mammalian cells. *Langmuir* **2001**, *17*, 6336−6343.
(52) Xiao, Y.; Truskey, G. A. Effect of receptor-ligand affinity on the strength of endothelial cell adhesion. *J. Biophys.* **1996**, *71*, 2869−2884.
(53) Livant, D. L.; Brabec, R. K.; Kurachi, K.; Allen, D. L.; Wu, Y.; Haaseth, R.; Andrews, P.; Ethier, S. P.; Markwart, S. The PHSRN Sequence Induces Extracellular Matrix Invasion and Accelerates Wound Healing in Obese Diabetic Mice. *J. Clin. Invest.* **2000**, *105*, 1537−1545.
(54) Kimura, K.; Hattori, A.; Usui, Y.; Kitazawa, K.; Naganuma, M.; Kawamoto, K.; Teranishi, S.; Nomizu, M.; Nishida, T. Stimulation of corneal epithelial migration by a synthetic peptide (PHSRN) corresponding to the second cell-binding site of fibronectin. *Invest. Ophthalmol. Vis. Sci.* **2007**, *48*, 1110−1118.
(55) Park, S.; Westcott, N.P.; Luo, W.; Dutta, D.; Yousaf, M.N. General chemoselective and redox-responsive ligation and release strategy. *Bioconjugate Chem.* **2014**, *25*, 543−551.
(56) Lamb, B.M.; Luo, W.; Nagdas, S.; Yousaf, M.N. Cell division orientation on biospecific peptide gradients. *ACS Appl. Mater. Interface* **2014**, *6*, 11523−11528.
(57) Lee, E.-J.; Chan, E. W. L.; Luo, W.; Yousaf, M.N. Ligand slope, density and affinity direct cell polarity and migration on molecular gradient surfaces. *RSC Adv.* **2014**, *4*, 31581−31588.
(58) Krabbenborg, S. O.; Huskens, J. Electrochemically Generated Gradients. *Angew. Chem., Int. Ed.* **2014**, *53*, 9152−9167.
(59) Gooding, J. J.; Parker, S. G.; Lu, Y.; Gaus, K. Molecularly engineered surfaces for cell biology: From static to dynamic surfaces. *Langmuir* **2014**, *30*, 3290−3302.
(60) Lee, J.; Choi, I.; Yeo, W.-S. Preparation of gradient surfaces by using a simple chemical reaction and investigation of cell adhesion on a two component gradient. *Chem.—Eur. J.* **2013**, *19*, 5609−5616.